中國機械工程學刊第三十九卷第二期第 171~178 頁(民國一百零七年)
Journal of the Chinese Society of Mechanical Engineers, Vol.39, No.2, pp 171~178 (2018)

Dynamic Characteristic and Experiment Analysis of Planetary Roller Screw

Jia-Nan Guo*, Peng He**, Zhan-Sheng Liu***, Hong-Yan Huang***, Yu-Ping Huang****and Wei-Tao Ding ****

Keywords: planetary roller screw, dynamic characteristics, contact analysis, experiment study.

ABSTRACT

This paper develops a dynamic model to predict the natural frequencies of planetary roller screw. In this model, meshing stiffness of planetary roller screw is taken into consideration. Based on this model, natural frequencies of the system with different mesh stiffness induced by variation of contact angle, roller radius and eccentricity are studied theoretically. The meshing stiffness and natural frequencies are found to increase with contact angle. The maximum natural frequencies reach peak values during the increase of the roller radius. The eccentricity leads to a non-uniform deflection of each roller around the screw. The eccentricity has little effect on the natural frequencies of planetary roller screw. Natural frequencies of the system are tested to valid the simulation results by setting up a planetary roller screw test rig. Comparisons between numerical and experimental results are presented and discussed.

INTRODUCTION

Planetary roller screw (PRS) is a type of high precision transmission device which is based on thread engagement. Most studies on PRS focus on kinetics characteristics and statics characteristics. Matthew et al. (2015) established a kinetic model and analyzed motion errors induced by roller slip. Yousef Hojjat et al. (2009) made an optimization for a PRS structure by changing the roller number and thread profile, and validated the optimized design by experiments. Aurégan et al. (2015) studied the tangential stress distribution of PRS and tested the roller slip under different lubrication conditions experimentally. Ma shangjun et al. (2013) studied the dynamic characteristics employing a finite element model. Matthew et al. (2014) built the earliest accurate statics stiffness model applying differential geometry method. Folly et al. (2016) proposed a new method to calculate the stiffness and statics load distribution, the results are verified by comparing with finite element method. In their further study (Folly A, 2016), they created a 3D finite element model of invert planetary roller screw. The axial stiffness is proved to be related with PRS structure parameters. Jin qianzhong et al. (1999) established a PRS axial stiffness model. Compared with ball screw, the stiffness of PRS is 50% higher. But the theory is aimed at ball screw structure and also brings in some error. They also made an experimental study on the relationship between friction and load (Jin Q. Z., 1998). Yang jiajun et al. (2011) established an axial stiffness model based on equivalent sphere theory and made a validation by experiments. Matthew et al. (2016) derived dynamic equation for PRS by involving in roller slip velocity and friction factors, making the equation too complex in spite of its accuracy. Yue Linlin (2014) built a 3D finite element model for PRS, and examined the first six orders natural frequency by a modal analysis. The disadvantage of this study is that it needs too much computation and time-consuming. There are few studies focused on the meshing stiffness model in PRS system. As the links in the whole transmission chain, meshing stiffness between threads determine the static and dynamic performance of the PRS. Thus, study about the calculation method for meshing stiffness is of great importance in PRS dynamic characteristic analyses.

This paper establishes a PRS dynamic model which takes the meshing stiffness into consideration. The first two order natural frequencies and modal shapes are achieved by simulation. The results show that the contact angle and roller radius have

Paper Received January, 2017. Revised April, 2017. Accepted April, 2017. Author for Correspondence: Jia-Nan Guo
**Ph.D student, Vibration and Acoustic Control Technology for Power Machinery, Harbin Institute of Technology, Harbin, 150001, China.*
***Lecturer, Vibration and Acoustic Control Technology for Power Machinery, Harbin Institute of Technology, Harbin, 150001, China.*
****Professor, Vibration and Acoustic Control Technology for Power Machinery, Harbin Institute of Technology, Harbin, 150001, China.*
*****Professor, China Academy of Launch Vehicle Technology, Beijing, 100000, China.*

significant influences on the first two order natural frequencies in investigated PRS system. A natural frequency experiment is set up to verify the accuracy of the simplified dynamic model.

DYNAMIC MODEL OF PRS

The PRS consists of a screw, rollers, a nut, a planetary carrier and ring gears, as given in Fig. 1. The screw is driven by motor. The rollers rotate around screw and the nut moves in a straight path together with rollers.

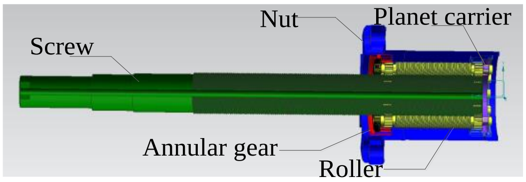

Fig. 1. The structure of PRS

During the working process, the load is acted on the nut. The rollers below screw provide support stiffness. The composite stiffness model of PRS is determined by body stiffness, thread stiffness and contact stiffness. The body stiffness and thread stiffness are along axial direction and the contact stiffness is vertical to the contact surface. There is a large number of thread contacts distributed in PRS making the PRS dynamic model complex. Thus, a simplified contact model of thread is given, as shown in Fig. 2. D_R is the diameter of roller; D_S is the diameter of screw; D_N is the diameter of nut; β is the contact angle between two contact bodies.

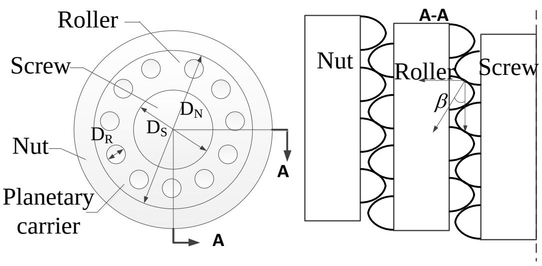

Fig. 2. Thread contact model

The support stiffness of PRS is the thread contact stiffness in vertical direction component. The deflection of two contact threads is listed (Johnson, 1985)

$$\delta = \left(\frac{9P^2}{16E^{*2}R_{Ei}} \right)^{\frac{1}{3}} \cos\beta F_2 \tag{1}$$

$$\frac{1}{E^*} = \frac{1}{E_1} + \frac{1}{E_2} \tag{2}$$

where P is the load acted on contact surface; E_1, E_2 are the modulus of elasticity of two contact surfaces; R_{Ei} is the equivalent radius of curvature; β is the contact angle; F_2 is the correction factor.

The equivalent radius of curvature is based on the equations below:

$$A + B = \frac{1}{2}\left(\frac{1}{R'} + \frac{1}{R''} \right) = \frac{1}{2}\left(\frac{1}{R_1'} + \frac{1}{R_2''} + \frac{1}{R_2'} + \frac{1}{R_2''} \right) \tag{3}$$

$$B - A = \frac{1}{2}\left\{ \begin{aligned} &\left(\frac{1}{R_1'} - \frac{1}{R_1''} \right)^2 + \left(\frac{1}{R_2'} - \frac{1}{R_2''} \right)^2 \\ &+2\left(\frac{1}{R_1'} - \frac{1}{R_1''} \right)\left(\frac{1}{R_2'} - \frac{1}{R_2''} \right) * \cos 2\gamma \end{aligned} \right\}^{\frac{1}{2}} \tag{4}$$

$$R_{Ei} = \frac{1}{2}(AB)^{-\frac{1}{2}} \tag{5}$$

where R_1' and R_1'' are the two principal radius of curvature of one contact body; R_2' and R_2'' are the two principal radius of curvature of another contact body; γ is the angle between the two principal curvature radii.

The stiffness of thread contact model between screw and roller is:

$$K_{HS} = \frac{F}{\delta_S} \tag{6}$$

where F is the load acted on screw and roller thread; K_{HS} is the stiffness of thread contact model between screw and roller; δ_S is the contact deflection of screw and roller.

One layer of thread contact stiffness for one roller consists of K_{HS} and K_{HN}. K_{HS} stands for the contact stiffness between roller and screw. K_{HN} stands for the contact stiffness between roller and nut. The two contact stiffness models are connected in series. The thread contact stiffness in the same thread layer for different rollers is in parallel.

$$K_H = \frac{K_{HS}K_{HN}}{K_{HS} + K_{HN}} \tag{7}$$

The contact stiffness increases non-linearly with the growth of contact angle. Fig. 3 presents the effect of contact angle on planetary roller screw axial stiffness. It shows that the contact stiffness increases with contact angle. The stiffness increases faster in high contact angle section.

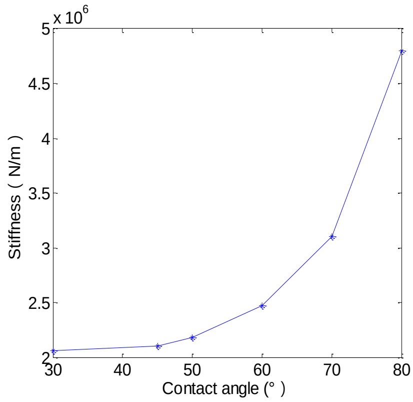

Fig. 3. Effect of contact angle on PRS axial stiffness

The parameters of the investigated PRS system are listed in Table 1.

Table 1 Parameters of PRS

Parameters	Value
Screw diameter/mm	21
Screw length/mm	256
Screw number of starts of thread	5
Screw helix angle/°	1.74
Nut diameter/mm	35
Nut length/mm	65
Nut number of starts of thread	5
Nut helix angle/°	1.04
Nut outside diameter/mm	54
Roller diameter/mm	7
Roller length/mm	30
Roller number	11
Roller thread number	75
Roller number of starts thread	1
Roller helix angle/°	1.04
Contact angle/°	45
Material	Cast steel

During the working process, the roller position is changing all the time. In this study, the roller position is shown as Fig. 4. The rollers are modeled as springs bearing only compressive force in vertical direction. This spring model is taken as the support stiffness model.

There are 11 rollers in this planetary roller screw, the angle between two rollers is 32.7˚. Roller deformation equations and equivalent stiffness in vertical component are listed:

$$\begin{cases} \delta_1 = \delta \times \cos\left(\dfrac{2\pi}{11} \times 2\right) \\ K_{H1} = \dfrac{F}{\delta_1} \end{cases} \tag{8}$$

$$\begin{cases} \delta_2 = \delta \times \cos\left(\dfrac{2\pi}{11}\right) \\ K_{H2} = \dfrac{F}{\delta_2} \end{cases} \tag{9}$$

$$\begin{cases} \delta_3 = \delta \times \cos(0) \\ K_{H3} = \dfrac{F}{\delta_3} \end{cases} \tag{10}$$

$$\begin{cases} \delta_4 = \delta \times \cos\left(\dfrac{2\pi}{11}\right) \\ K_{H4} = \dfrac{F}{\delta_4} \end{cases} \tag{11}$$

$$\begin{cases} \delta_5 = \delta \times \cos\left(\dfrac{2\pi}{11} \times 2\right) \\ K_{H5} = \dfrac{F}{\delta_5} \end{cases} \tag{12}$$

$$K = K_{H1} + K_{H2} + K_{H3} + K_{H4} + K_{H5} \tag{13}$$

where δ is the deflection of each roller; δ_1 is the deflection of roller 1 in vertical direction; K_{H1} is the vertical stiffness of roller 1; K is the support stiffness of planetary roller screw; F is the force act on the roller.

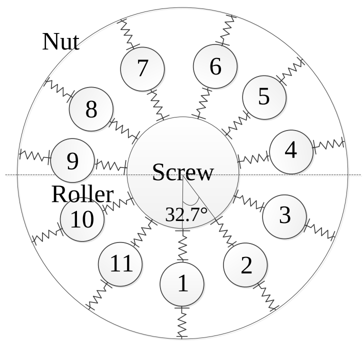

Fig. 4. The roller distribution of simplified PRS

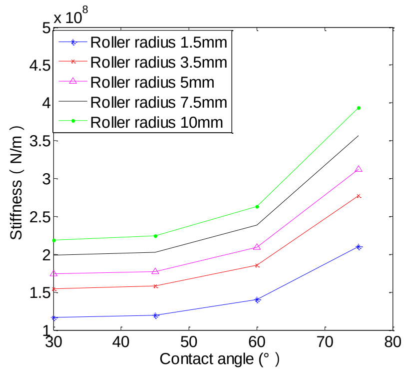

Fig. 5. Effect of contact angle on PRS supporting stiffness

Fig. 5 presents the effect of contact angle on PRS supporting stiffness. It shows the supporting stiffness increases with contact angle and it grows faster as the contact angle increases.

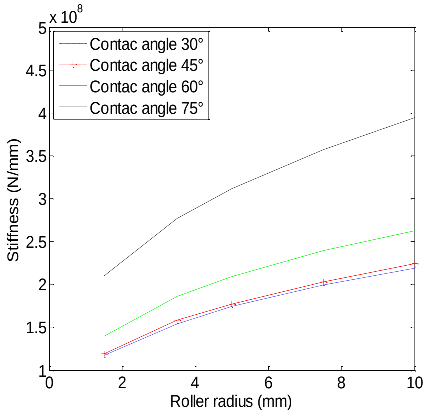

Fig. 6. Effect of roller radius on PRS bracing stiffness

Fig. 6 shows the effect of roller radius on PRS supporting stiffness. The curves show the supporting stiffness increases with roller radius. The supporting stiffness tends to a limit under different contact angles. The roller radius is associated with the roller thread profile and the curvature radius (Matthew, 2014). The increase of roller radius leads to a growth of curvature radius which will cause a growth of contact stiffness.

The screw is simplified as a beam. And the nut and rollers are discretized as springs and added mass element which are connected with the screw. The simplified structure of PRS scheme is shown as Fig. 7.

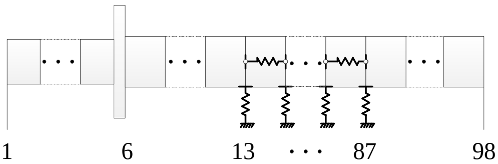

Fig. 7. A simplified model of PRS

The planetary roller screw is settled horizontally. To be consistent with the experiment, the planetary roller screw is discretized into 97 solid elements, 75 spring elements and 75 added mass elements. The spring elements and added mass elements are placed from node 13 to node 87 which represent the nut, rollers and the thread contact stiffness. The dynamic equation of planetary roller screw is listed:

$$[M]\{\ddot{u}\}+[C]\{\dot{u}\}+[K]\{u\}=\{Q\} \tag{14}$$

The relationship between the modal frequency and the modal shape is listed:

$$\{-[M]\omega_r^2+[K]\}\{\phi^{(r)}\}=\{Q\} \tag{15}$$

where *[M]* is the mass matrix with the dimension of 490×490; *[K]* is the stiffness matrix with the dimension of 490×490 which consists of bending rigidity and the nonlinear supporting stiffness; *{Q}* is the system load; *{u}* is the displacement of the system with the dimension of 490×1 which consists of bending displacement, axial displacement, and the bending angle of two directions, $\{u\}=[x_1, y_1, z_1, \theta x_1, \theta y_1, \ldots, x_{98}, y_{98}, z_{98}, \theta_{x98}, \theta_{y98}]$; ω_r is the modal frequency; $\{\varphi^{(r)}\}$ is the corresponding modal shape.

THE PRS NATURAL FREQUENCY SIMULATION

The simulation of the first and second natural frequency of planetary roller screw is conducted based on the simplified dynamic model. The first and second order vibration shapes are given in Fig. 8 and Fig. 9.

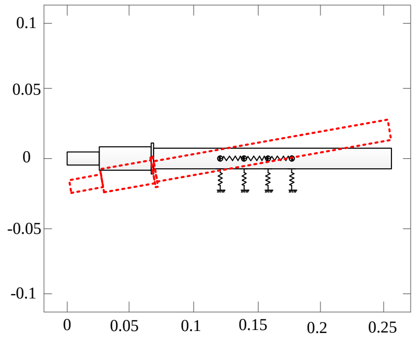

Fig. 8. The first-order vibrating modal of PRS

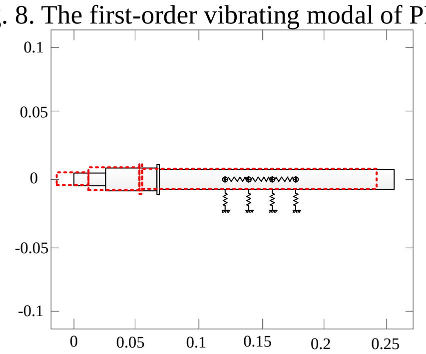

Fig. 9. The second-order vibrating modal of PRS

According to the graphs of vibration, Fig. 8 is the first-order vibration model which shows that there is a large displacement on both axial and radial direction. Fig. 9 is the second-order vibration model which shows the axial movement. The vertical axis is the axial movement of screw in Fig. 9. The result of natural frequencies simulation shows the first-order natural frequency of PRS is 182Hz and the second-order natural frequency is 781Hz.

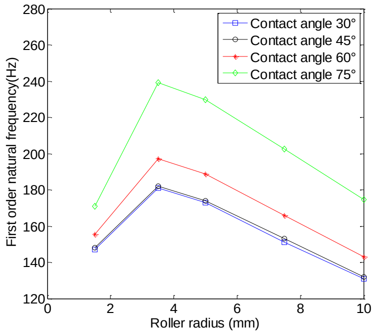

Fig. 10. Effect of roller radius on PRS first natural frequency

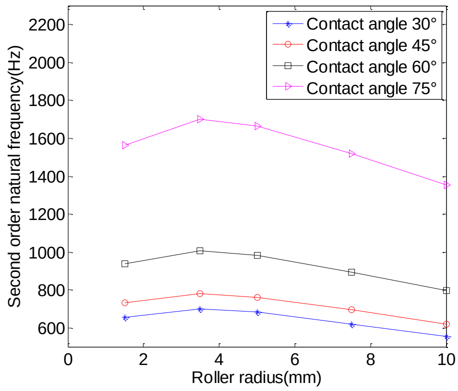

Fig. 11. Effect of roller radius on PRS second natural frequency

The contact angle and roller radius have a great influence on supporting stiffness, leading to a great impact on natural frequency. In the simulations above, the length of screw keeps constant. According to Fig. 10 and Fig. 11, it shows the influence of roller radius is not monotonic increasing. The maximum values of first and second natural frequencies are achieved at 3.5mm of roller radius. The increase of roller radius leads to not only an increase of supporting stiffness, but also an increase of rotational inertia.

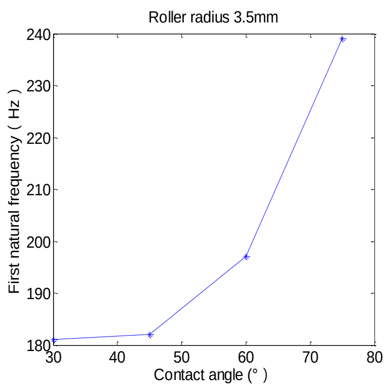

Fig. 12. Effect of contact angle on PRS first natural frequency

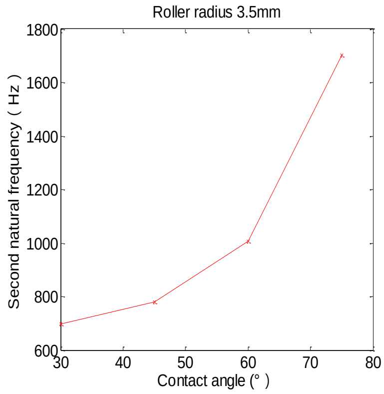

Fig. 13. Effect of contact angle on PRS second natural frequency

Fig. 12 and Fig. 13 are the effect of contact angle on planetary roller screw first and second natural frequency. This roller radius in this simulation is 3.5mm. The result shows that the first and second natural frequency increases with the contact angle.

Fig. 14 is the eccentricity distribution for 11 rollers. The maximum eccentricity is 0.09mm which exists on roller 1 as in Fig. 14. The minimum value of eccentricity exists on roller 6 and roller 7.

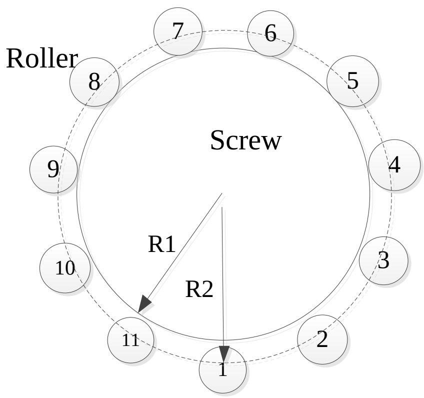

Fig. 14. The eccentricity distribution of planetary roller screw

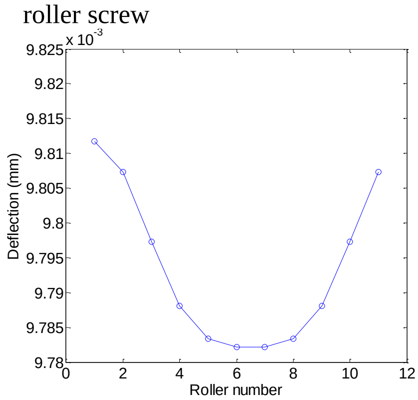

Fig. 15. The deflection for rollers

Fig. 15 shows the deflection changes with roller number under the force of 15000N. Roller 1 has the maximum deflection. Roller 6 and roller 7 have the minimum deflection. The deflection has the same variation tendency with eccentricity. The first and second order natural frequencies are also influenced by eccentricity as shown in Fig. 16 and Fig. 17.

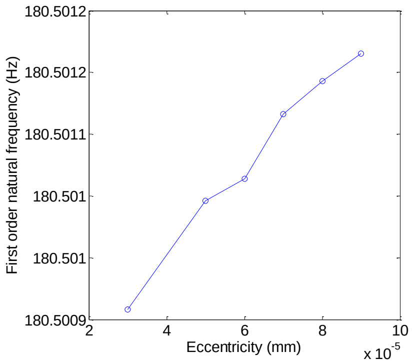

Fig. 16. Effect of eccentricity on first order natural frequency

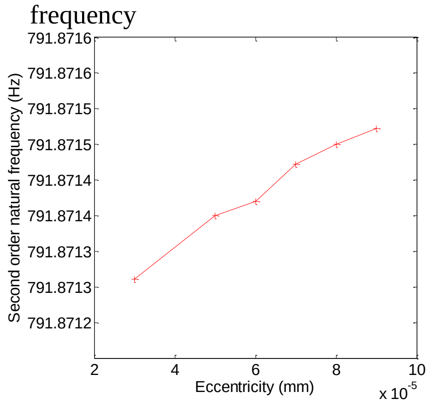

Fig. 17. Effect of eccentricity on second order natural frequency

Due to the existence of the eccentricity, the contact angle and thread stiffness are deviated from the ideal case. The small eccentricity leads to little variations of the contact angle and thread stiffness. Thus, the variation of the frequency is not very obvious.

THE PRS NATURAL FREQUENCY EXPERIMENT

An experiment test is set up to evaluate the planetary roller screw natural frequency. Fig. 18 is the PRS natural frequency experiment schematic diagram.

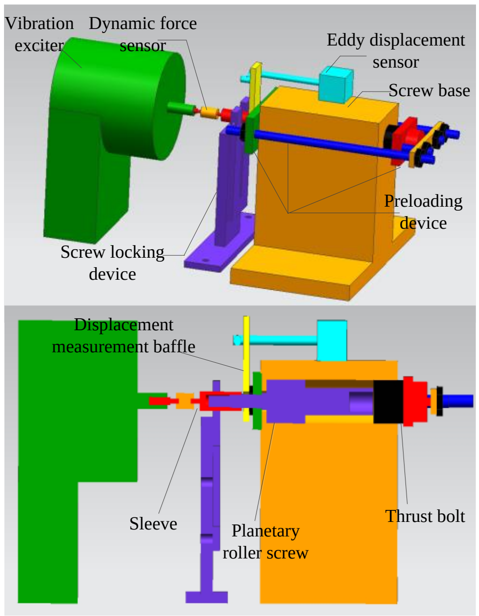

Fig. 18. Diagram of planetary roller screw natural frequency experiment

The experiment devices consist of vibration exciter, planetary roller screw, screw base, dynamic force sensor, eddy displacement sensor, preloading device, screw locking device, data acquisition and analysis system. The vibration exciter is connected to screw along axial direction. The preloading device provides preload to screw. The PRS is installed in screw base. Screw base is a cuboid body, the material is A283-D. The screw locking device is used to provide torsional constrain for the screw. The thrust bolt is used to provide axial constrain for the nut. The thrust bolt diameter is 54mm and the length is 50mm. The experiment system is shown in Fig. 19.

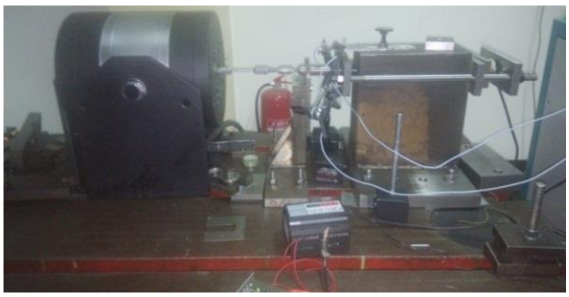

Fig. 19. Planetary roller screw natural frequency experiment

Table 2 is the parameters of sensors used in this experiment. The parameters of the dynamic experiment test bed are listed in Table 3.

Table 2 Parameters of sensors

Sensor	Work scope	Sensitivity
Dynamic force sensor	0-5000N	4pC/N
Eddy displacement sensor	0-1mm	0.0625mm/V

Table 3 Parameters of natural frequency experiment device

Part	Length(mm)	Width(mm)	Height(mm)
Screw base	400	240	300
Screw locking device	400	90	300

Fig. 20 and Fig. 21 are the time history diagrams of screw displacement and vibration force. The vibration force applied by vibration exciter is sine force. Fig. 22 presents the result of frequency response analysis by data acquisition and analysis system. It shows that there are two obvious vibrations on 195Hz and 747Hz. These are the first two natural frequencies.

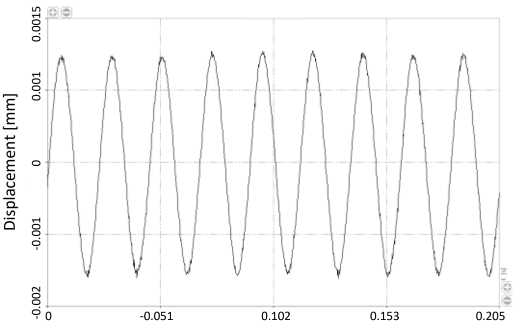

Fig. 20. Time history diagram of displacement

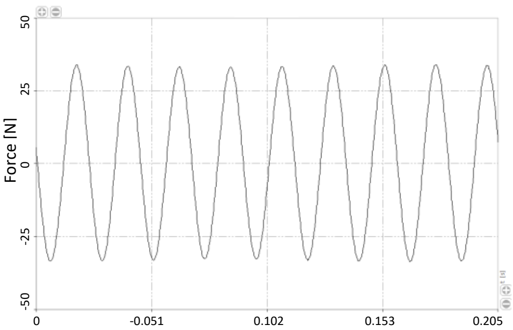

Fig. 21. Time history diagram of force

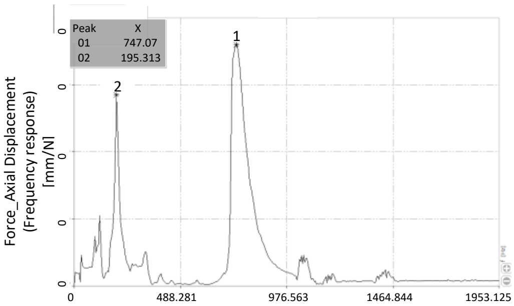

Fig. 22. Frequency response analysis of PRS natural frequency experiment

By varying the excitation frequency, the relationship between vibration force and PRS deformation is achieved. The first two natural frequencies are achieved by using frequency response analysis. The thread contact surface is a slope. So the axial vibration force applied by vibration exciter creates both radial force and axial force. It will generate both axial displacement and radial displacement of the system members. The experiment result shows the first natural frequency is 195Hz and the second natural frequency is 747Hz. The error between experiment results and simulation results are 6.7% and 4.3%. Clearances between contact surfaces contribute to these errors. The comparison between experiment result and simulation result verified the accuracy of the dynamic model presented in this paper.

CONCLUSION

This paper establishes a planetary roller screw dynamic model which takes the thread engagement into consideration and carries out a PRS natural frequency experiment.

(1)The influences of thread contact angle and roller radius are discussed. The results show the meshing stiffness increases with contact angle and roller radius.

(2)The first two natural frequencies and modal shapes are achieved by a simplified dynamic model of PRS. The first-order natural frequency is 182Hz and the second-order natural frequency is 781Hz.

(3)A natural frequency experiment is set up to verify the simulation results. The comparison shows the two results are quite close. The errors of the two natural frequencies are less than 6.7%. This shows the dynamic model is accurate.

(4)The analysis result shows the first two natural frequencies increase with contact angle. The first two natural frequencies reach the maximum while the roller radius is 3.5mm in the investigated PRS system.

(5)The eccentricity leads to a non-uniform deflection for different roller. It also causes a variation of the first and second order natural frequency in the PRS system. Thus, the effects of eccentricity on natural frequency are not significant, which shows a high transmission accuracy of the PRS.

This work provides a reference for the dynamic modeling method for actuator system of aero-craft. In the future studies, friction and wear factors will be involved in to examine the dynamic characteristics of the PRS system.

ACKNOWLEDGEMENT

The authors gratefully acknowledge the Institute of Vibration and Acoustic Control Technology for Power Machinery for its grant and support. This work was performed under a Ph.D. dissertation contract at Harbin Institute of Technology, China.

REFERENCES

Folly A., Alain D., Michel C., et al. "Static Load Distribution and Axial Stiffness in a Planetary Roller Screw Mechanism," Journal of Mechanical Design, Vol. 138, No. 1, pp.012301-1~11(2016).

Folly A., Alain D., Michel C., et al. "Static Analysis of an Inverted Planetary Roller Screw Mechanism," Journal of Mechanism and Robotics, Vol. 8, No. 4, pp.041020-1~14(2016).

G. Aurégan, V. Fridrici, Ph. Kapsa, et al.. "Experimental simulation of rolling-sliding contact for application to planetary roller screw mechanism," Wear, Vol. 332, pp. 1176-1184(2015).

Jin Q. Z., Yang J. J., Sun J. L., "The comparative research on the static stiffness of ball screw and planetary roller screw," Mechanical Science and Technology, Vol. 8, No. 2, pp.230-232(1999).

Jin Q. Z., Yang J. J., Sun J. L., "The research on friction mechanism of the planetary roller screw," Journal of Huazhong University of Science and Technology, Vol. 26, No. 6, pp. 82-96 (1998).

Johnson K. *Contact Mechanics*. Cambridge University Press, UK(1985).

Ma S. J., Liu G., Zhou J. X., et all. "Dynamic characteristic analysis of a planetary roller screw in operating process," Journal of Vibration and Shock, Vol. 32, No. 3, pp.167-171(2013).

Matthew H. J., Steven A. "Stiffness of roller screw mechanism by the direct method," Mechanics based design of structures and machines, Vol. 42, No. 1, pp.17-34(2014).

Matthew H. J., Steven A., Ty A. Lasky, "Dynamics of the Planetary Roller Screw Mechanism," Journal of Mechanisms and Robotics, Vol. 8, No. 1, pp.1-19(2016).

Matthew H. J, Steven A. V. "Kinematics of roller migration in the planetary roller screw mechanism," Journal of Mechanical Design, Vol. 131, pp.134 (2015).

Yang J. J., Wei Z. X., Zhu J. S, et al. "Calculation of load distribution of planetary roller screws and static rigidity," Journal of Huazhong University of Science and Technology, Vol. 39, No. 4, pp.1-4(2011).

Yehezkely E., Karpel M. "Nonlinear flutter analysis of missiles with pneumatic fin actuators," Journal of Guidance Control and Dynamics, Vol. 19, No.3, pp.664-670 (1996).

Yousef Hojjat, M Mahdi Agheli. "A comprehensive study on capabilities and limitations of roller–screw with emphasis on slip tendency," Mechanism and Machine Theory, Vol. 44, pp.1889-1899 (2009) .

Yue L. L., Wang W. Y., Hu B. G., "Dynamic Characteristic Analysis Based on Finite Element Simulation for Planetary Roller Screw," Vol. 183, No. 2, pp.16-18(2014).

NOMENCLATURE

A ,B : Constant to calculate equivalent radius
E : Modulus of elasticity
F: Load on each thread
F_2 *:* Correction factor
K_{Hi}: Contact stiffness for body i
P : Load on contact surface
Q: System load
R_i', R_i'': First and second principal radius of curvature for body i
R_{Ei} : Hertzian equivalent radius
β: Contact angle
γ: Angle between two principal curvature radii
δ: Contact deflection
δ_i: Deflection of a body i in vertical direction.
ω_r : Modal frequency
[M]: System mass matrix
[K]: System stiffness matrix
[C]: System damping matrix
$\{\varphi^{(r)}\}$: Modal shape

行星滾柱絲杠動力學特性分析及試驗研究

郭嘉楠 何鵬 劉佔生 黃洪雁
哈爾濱工業大學動力機械振動與噪聲控制技術研究所

黃玉平 丁偉濤
北京精密機電控制設備研究所

摘 要

本文建立了考慮嚙合剛度的行星滾柱絲杠動力學模型。分析了接觸角、滾柱半徑和偏心對嚙合剛度以及行星滾柱絲杠固有頻率的影響規律：行星滾柱絲杠的嚙合剛度和固有頻率都隨著接觸角的增加而增大。滾柱半徑達到某一特定值時行星滾柱絲杠固有頻率達到最大。偏心會導致圍繞在絲杠周圍的滾柱產生不均勻的變形，但其對行星滾柱絲杠的固有頻率的影響較小。搭建行星滾柱絲杠固有頻率特性試驗台，驗證了模擬計算結果的準確性。